Submillimeter wave vibration–rotation spectroscopy of $Ar \cdot CO$ and $Ar \cdot ND_3$

Dmitry G. Melnik, Sandhya Gopalakrishnan, Terry A. Miller, Frank C. De Lucia, and Sergey Belov

Citation: The Journal of Chemical Physics **114**, 6100 (2001);
View online: https://doi.org/10.1063/1.1355660
View Table of Contents: http://aip.scitation.org/toc/jcp/114/14
Published by the American Institute of Physics

Submillimeter wave vibration–rotation spectroscopy of Ar·CO and Ar·ND_3

Dmitry G. Melnik, Sandhya Gopalakrishnan, and Terry A. Miller
Department of Chemistry, The Ohio State University, 120 W. 18th Avenue, Columbus, Ohio 43210

Frank C. De Lucia
Department of Physics, 174 W.18th Avenue, Columbus, Ohio 43210

Sergey Belov
Institute of Applied Physics of RAS, 46 Ulyanova Str., Nishny Novgorod 603600, Russia

(Received 8 December 2000; accepted 24 January 2001)

A new absorption spectrometer operating in the submillimeter wave region has been designed. The apparatus combines the previously reported fast scan submillimeter wave spectroscopic technique (FASSST) and a pulsed supersonic jet sample. It is specially designed for the rapid searching for unknown molecular transitions of weakly absorbing and/or low abundance species. Vibration–rotation transitions of the Ar·CO and Ar·ND_3 van der Waals molecules have been observed using this apparatus. Transitions in Ar·CO involve the $j=1\rightarrow j=2$ hindered rotor transition in the complex. Transitions in Ar·ND_3 have been assigned as the rotational structure of the fundamental of the lowest frequency bending mode involving the two moieties. Transitions have been observed emanating from the levels correlating to the two lowest energy inversion components of ND_3 yielding a determination of the inversion splitting in the complex. © *2001 American Institute of Physics.* [DOI: 10.1063/1.1355660]

I. INTRODUCTION

Although a subject of important research interest for many years, the submillimeter wave spectral region retains great potential for exploration particularly because of the increasing availability of powerful sources of radiation continuously covering the region to ever higher frequencies. Spectroscopy in this region can give important information about types of molecular motion that is unavailable from other techniques. These molecular motions include low frequency large amplitude vibrations, vibration-tunneling-rotation (VTR), and internal rotation and/or pseudorotation. Submillimeter spectroscopy makes it possible to observe the transitions involving these motions directly and measure them with higher accuracy and resolution than can be done with conventional infrared and electronic spectroscopy.

The present work has been performed with an apparatus that combines the FASSST spectroscopic method described elsewhere[1] with a pulsed supersonic free jet. Real-time absolute frequency monitoring is introduced to implement the FASSST technique in a pulsed mode. The jet cooled environment facilitates the production of van der Waals complexes. The use of the free supersonic jet also leads to rotational cooling of the probed molecules and significantly reduces spectral congestion. Additionally, the reduction of the rotational partition function increases the absorption signal for the remaining transitions, thereby compensating for the reduction in absorption path length with respect to conventional submillimeter wave spectroscopy. The initial use of the apparatus was to observe the rotational spectrum of the Ar·CO cluster which is an ideal test molecule since it is both weakly absorbing and a low abundance species. The experimental data we obtained are in good agreement with frequencies predicted from the molecular constants recently reported by Hepp *et al.*[2]

The apparatus has been used more extensively to study VTR transitions of Ar·ND_3. The Ar·NH_3 complex has been studied in the past.[3–14] Based on these results Schmuttenmaer *et al.* calculated a potential energy surface (PES) for this complex[4] and used it to predict the energies of a number of levels of the perdeuterated complex. These predictions indicate that there is an Ar·ND_3 bending vibrational transition that originates in the ground vibrational state of Ar·ND_3 and which should lie within the spectral range presently accessible to the apparatus. An important advantage of observing transitions in Ar·ND_3 is that they yield the possibility of measuring the inversion splitting in $k=0$ states, associated with the ND_3 subunit of the complex, where unlike NH_3 both inversion levels have nonzero spin statistical weights. The observation of inversion in the complex potentially provides important information about the PES that was not derived from the Ar·NH_3 experiments.

II. EXPERIMENT

The apparatus uses a free running backward wave oscillator (BWO) tube (ISTOK Research Company, Russia) driven by a high voltage sweeper to produce rapidly tunable submillimeter wave radiation. In the present work, an OB-24 tube was used, with a spectrum range of 167–263 GHz. As the block diagram of the apparatus (Fig. 1) illustrates, the output of the BWO is split into two beams. One of the beams, carrying 80–90 % of the power, is focused onto the molecular jet produced by a pulsed valve (General Valve,

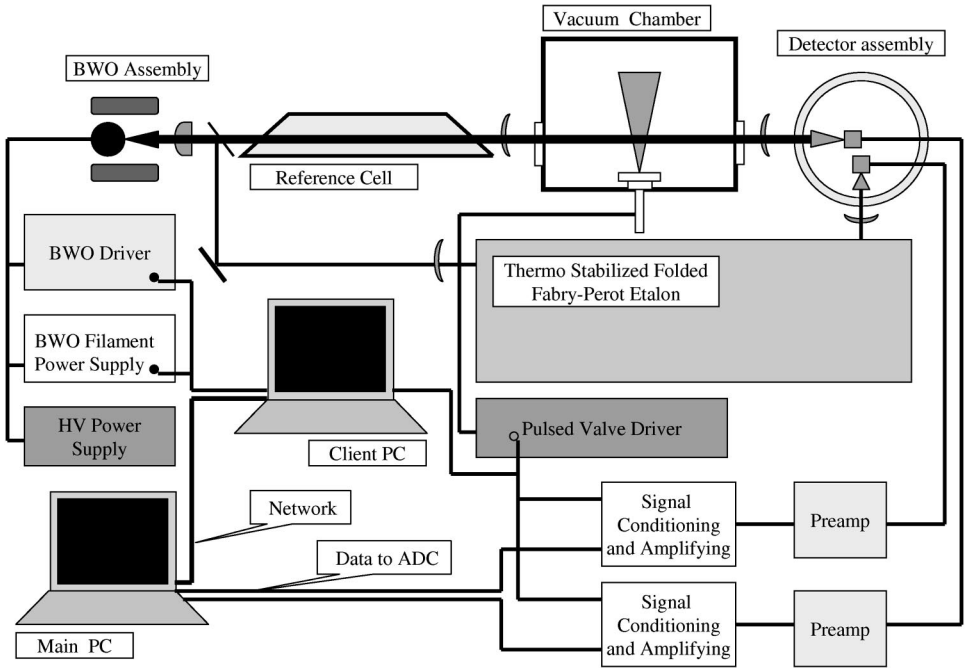

FIG. 1. Schematic diagram of the FASSST-pulsed jet spectrometer.

model 9), and is detected by a hot electron InSb bolometer (QMC Instruments) mounted in a liquid helium cooled Dewar (Microwave Laboratories). The electrical signal produced by the bolometer, amplified by a low noise battery-powered preamplifier (QMC Instruments, model ULN 95) is the data channel. A low pressure (about 0.1 Torr) absorption cell is also inserted into this beam. The cell contains molecules (e.g., OCS) whose known transitions provide absolute frequency markers. Thus, the data channel contains both the spectrum of the sample and that of reference molecules. The spectral signal is amplified, filtered, and fed to a fast ADC board (Computer Boards, model 9812) installed in the main computer which collects data and stores it on a local hard drive.

The second beam is directed through a thermally stabilized folded Fabry–Perot cell that produces fringes with a free spectral range of 14.475 MHz. This beam is detected by a second bolometer mounted in the same Dewar as the signal detector. The output of this channel is recorded simultaneously with the data channel and processed to generate digital frequency markers for relative frequency calibration.

These markers are fed to a client computer running real-time software, that provides a low level control. The client computer has no user interface and is interfaced to the main computer through a custom-made network as illustrated in Fig. 1. The software the client is running allows it to alternatively serve as a pulse counter, delay generator or interface link to different parts of the apparatus. As an interface device, it handles digital input from both acquisition channels and the BWO driver, and digital output to the pulsed valve driver and acquisition system. The BWO driver provides a digital output signal at the turning points of a sawtooth voltage ramp which serves as a master clock for each operational cycle of the spectrometer. After reception of the master clock signal, a fairly narrow spectral window (about 250 MHz) is chosen, wherein only one molecular reference line appears.

The desired frequency for the commencement of data taking is determined by counting the number of Fabry–Perot markers after the reception of the molecular reference frequency marker. To ensure proper synchronization between the pulsed valve and the data acquisition trigger, the valve is triggered before the data acquisition hardware. Once the molecular reference marker is received, the client computer operates as a pulse counter. Therefore, the valve, as well as the data acquisition hardware, is triggered after appropriate delays, which are determined by counting fringe markers.

Data acquisition only occurs while the frequency is being scanned with the valve open. A given interval of this nature is called a data frame. The typical opening duration of the valve is about 2 milliseconds, which results in data frames of 200–300 MHz with hardware-limited resolution of 50–75 kHz (and minimum linewidths of $\approx$300 kHz limited by Doppler broadening due to the shape of the jet expansion).

To increase sensitivity and signal-to-noise ratio, two amplifiers with adjustable bandwidth (PARC preamplifiers, model 113) perform bandwidth narrowing (roll-off). Data is taken by recording pairs of traces with the valve, respectively, opened and closed, followed by subtraction of the latter trace from the former, with the result being stored in the main computer. This approach eliminates molecular absorption in the reference cell from the data. It also minimizes the effect of frequency-dependent fluctuations of the submillimeter wave radiation reaching the detector. Signal averaging is performed to further improve the spectra.

In the Ar·CO experiments a pre-mixed sample of 13% of CO (99.9% carbonyl free grade), 17% of Ar (99.998% grade) in helium (99.99% grade) was expanded through a pinhole nozzle 0.5 mm in diameter at backing pressures of 40–55 psi.

In the Ar–ND_3 experiment, a pre-mixed sample of 1% of ND_3 and 20% of Ar diluted in helium was used. The

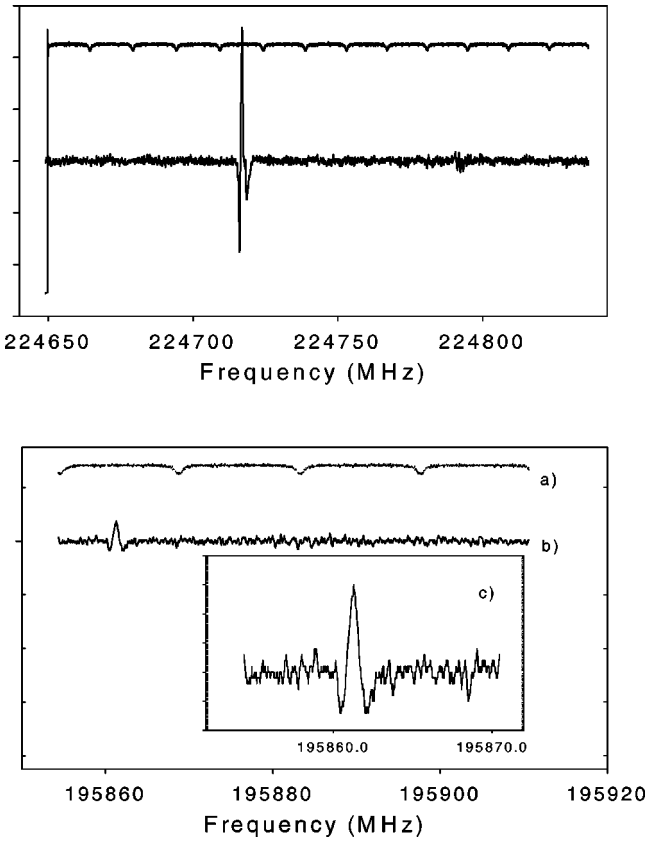

FIG. 2. Top, the $J=1\rightarrow J=2$ rotational transition in $^{12}C^{17}O$ at a concentration of 100 ppm in the jet with an integration time of 400 μs; the upper trace shows the frequency markers generated by the Fabry–Perot cell. On the bottom, the $Q_2(6)$ rotational transition in Ar–CO, taken with the same integration time; trace (c) shows the transition on an enlarged scale and trace (a) the frequency markers.

perdeuterated ammonia was purchased from Aldrich Chemical Company (99 atom % D grade), and argon from AGA (99.998% grade); 99.99% helium was used as a buffer gas. Both slit and circular nozzles were used. The slit nozzle is made by fixing atop a 0.75 mm General Valve a special adapter with a slit 18 mm long and 12 to 25 micron wide. For the circular expansion, a 0.5 mm pinhole fixture was used. The pressure behind the expansion was varied between 30 and 50 psi. The typical temperature of the sampled molecules as determined from the rotational spectrum was about 10 K. In all experiments, the mixture was expanded into a vacuum chamber pumped by a Roots pump (Leybold–Heraeus, WS250) backed by a mechanical pump.

III. RESULTS AND DISCUSSION

A. Ar·CO

The sensitivity of the apparatus was tested by observing transitions in CO isotopomers and the Ar·CO van der Waals complex. Figure 2 shows typical traces of the transitions observed. The trace of a rotational transition corresponding to $J=1\rightarrow J=2$ in $^{12}C^{17}O$ in natural abundance (Fig. 2, top) has been taken in a supersonic jet formed by expanding a 50% mixture of CO in helium through a circular orifice 0.5 mm in diameter yielding an estimated rotational temperature of about 20 K. From the measurements of CO isotopomers it was concluded that the apparatus is capable of detecting the weak absorber CO (permanent dipole moment 0.11 Debye) at concentrations of about 10 ppm with integration time of 400 μs per data point. The transitions in the Ar·CO complex were observed in the range of 195–220 GHz. The trace of $Q_2(6)$ is shown on Fig. 2, bottom. A total of 18 transitions were observed and their frequencies are given in the Table I.

TABLE I. Experimentally observed transitions in Ar·CO.[a]

Transition	Obs. freq (MHz)	Pred. freq (MHz)	Obs.–Pred. (MHz)
$Q_1(3)$	195 627.8	195 627.5	0.3
$Q_1(4)$	195 690.0	195 690.3	−0.3
$Q_1(5)$	195 767.7	195 768.2	−0.5
$Q_1(6)$	195 861.3	195 861.0	0.3
$Q_1(7)$	195 969.0	195 968.2	0.8
$R_1(1)$	203 694.6	203 694.9	−0.3
$R_2(1)$	203 565.5	203 565.9	−0.4
$R_1(2)$	207 794.3	207 793.8	0.5
$R_2(2)$	207 408.9	207 407.8	1.1
$R_1(3)$	211 900.6	211 900.0	0.6
$R_2(3)$	211 131.8	211 130.8	1.0
$R_1(4)$	216 008.6	216 009.1	−0.5
$R_2(4)$	214 732.5	214 732.6	−0.1
$R_1(5)$	220 115.7	220 116.0	−0.3
$R_2(5)$	218 210.0	218 210.9	−0.9
$R_1(6)$	224 214.6	224 214.0	0.6
$R_2(6)$	221 563.2	221 563.3	−0.1
$R_1(7)$	224 787.2	224 786.9	0.3

[a]For details of the prediction, see text.

The frequencies of the observed Ar·CO transitions were compared to the frequencies predicted using the semi-rigid Hamiltonian used by Xu *et al.*,[15] with the corrections and molecular constants reported by Hepp *et al.*[16] The results of the comparison of predicted and experimental values are shown in Table I.

B. Ar·ND_3

1. Theoretical considerations

ND_3 is an oblate symmetric top belonging[3] to the PI group $D_{3h}(M)$ which is isomorphic with the point group D_{3h}. The expected energy level pattern is shown in Fig. 3(a) which also labels the energy levels by the total angular momentum quantum number j and its projection on the C_{3v} axis, k. We choose lower case letters to denote the quantum numbers of the ND_3 moiety and upper case letters for the quantum numbers of the complex. ND_3 exists, for the purposes of this experiment, in two inconvertible forms distinguished by different total nuclear spin.

Each j_k state of ND_3 is split by the inversion-tunneling into a symmetric and antisymmetric state [designated as + and −, respectively, in Fig. 3(a)]. The inversion splitting between symmetric and antisymmetric states is ΔV and equals 1591.8 MHz in the vibrationless ND_3 molecule.[17]

For $k=0$ the mapping of the ND_3 energy level structure of Ar·ND_3 is given in Fig. 3(b). Following the notation of Schmuttenmaer *et al.*,[3,4] the energy levels of the complex are correlated with that of the free ammonia molecule and designated as Σj_k, Πj_k, etc., where Σ corresponds to $\Omega=0$,Π to $\Omega=1$. Ω denotes the projection of the complex

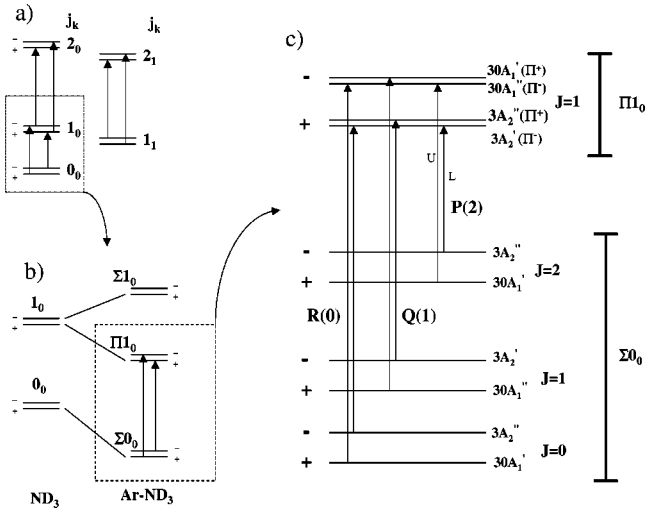

FIG. 3. Energy level and transition diagram for ND_3 and $Ar\cdot ND_3$: (a) energy levels in monomer; (b) correlation between the energy levels in ND_3 and $Ar\cdot ND_3$; (c) Π-bend transition in $Ar\cdot ND_3$. Energy levels include overall rotation of the complex. The full rovibrational–inversional symmetry (A_1', etc.) is indicated, with the numbers preceding indicating the nuclear spin statistical weight. ''+'' and ''−'' signs label inversion levels. In case of $Ar\cdot ND_3$ these signs are not rigorous quantum numbers but indicate correlation with the corresponding symmetry components in monomer. *L* and *U* label transitions corresponding to the lower and the upper frequency inversion components, respectively, of the band.

total angular momentum **J** on the van der Waals bond, with the *j* and *k* quantum numbers correlating with the corresponding states of free ND_3.

The basis functions for the complex may be chosen as products of a radial stretching function, $|n\rangle$, between the moieties, an angular function representing the torsional–rotational motion $|j,k,J,\Omega,M\rangle$, an inversion function, $|\rho\rangle$, and a nuclear spin function Ψ_{NS}. Thus $\Psi_{\text{total}}=\Psi_S\cdot\Psi_{NS}$, where $\Psi_S=|n\rangle|j,k,J,\Omega,M\rangle|\rho\rangle$ is the spatial part of a wave function.

We now consider the effect of the symmetry operations of the group D_{3h} PI on Ψ_S. The radial function $|n\rangle$ is symmetric under the symmetry operations since both states involved in the observed transition have zero quanta of van der Waals stretch. The effect of the symmetry operations on the torsional–rotational part, $|j,k,J,\Omega,M\rangle$, of the function have been previously published[6] and are summarized in Table II. Using these results, we see that new basis functions transforming as irreducible representations of the PI group can be written such that $\Psi_S=|n\rangle\cdot\Psi_{tr}\cdot|\rho\rangle$, where Ψ_{tr} is one of the symmetrized functions

TABLE II. The effect of the operations of PI D_{3h} group on basis set $|jk\Omega JM\rangle$.

Operation	Effect on basis
E	$\lvert jk\Omega JM\rangle$
(123)	$\exp(2\pi ik/3)\lvert jk\Omega JM\rangle$
(23)*	$(-1)^{J+k}\lvert j\text{-}k\text{-}\Omega JM\rangle$
E*	$(-1)^{J+j+k}\lvert jk\text{-}\Omega JM\rangle$
(123)*	$(-1)^{J+j+k}\exp(2\pi ik/3)\lvert jk\text{-}\Omega JM\rangle$
(23)	$(-1)^{j}\lvert j\text{-}k\Omega JM\rangle$

$$|++\rangle=1/2[(|jkJ\Omega M\rangle+|j-kJ\Omega M\rangle)+(|jkJ-\Omega M\rangle+|j-kJ-\Omega M\rangle)], \quad (1a)$$

$$|-+\rangle=1/2[(|jkJ\Omega M\rangle-|j-kJ\Omega M\rangle)+(|jkJ-\Omega M\rangle-|j-kJ-\Omega M\rangle)], \quad (1b)$$

$$|+-\rangle=1/2[(|jkJ\Omega M\rangle+|j-kJ\Omega M\rangle)-(|jkJ-\Omega M\rangle+|j-kJ-\Omega M\rangle)], \quad (1c)$$

$$|--\rangle=1/2[(|jkJ\Omega M\rangle-|j-kJ\Omega M\rangle)-(|jkJ-\Omega M\rangle-|j-kJ-\Omega M\rangle)]. \quad (1d)$$

In case of $k=0$, functions (1b) and (1d) vanish. Furthermore, for the $\Sigma 0_0$ state ($\Omega=0$), only the $|++\rangle$ state exists for each *J*. For the $\Pi 1_0$ state, there are two nonvanishing wave functions for each *J* ($|++\rangle$ and $|+-\rangle$) which are split by Coriolis interaction with the upper $\Sigma 1_0$ state. The lower Coriolis component, pushed down by the interaction, is denoted as Π^- and the other, unaffected one is denoted as Π^+ (see Fig. 3). The direct application of the transformation properties given in Table I to the symmetrized wave functions Ψ_{tr} reveals the following symmetry properties of the torsional–rotational functions.

In the $\Sigma 0_0$ state:

$|++\rangle$ transforms as A_1' and A_1'' for even and odd *J*, respectively.

In the $\Pi 1_0$ state:

$|++\rangle$ transforms as A_2'' and A_2' for even and odd *J*, respectively, and

$|+-\rangle$ transforms as A_2' and A_2'' for even and odd *J*, respectively.

The inversion wave functions $|\rho\rangle$ associated with the states labeled ''+'' and ''−'' in Fig. 3 transform, respectively, as A_1' and A_2'' irreducible representations in the D_{3h} group.[18]

The direct product

$$\Gamma(\Psi_S)=\Gamma(|\rho\rangle)\cdot\Gamma(\Psi_{tr})\cdot\Gamma(|n\rangle) \quad (3)$$

of the irreducible representations for $|\rho\rangle$ and $|n\rangle$ and Ψ_{tr} gives the symmetries of Ψ_S that are shown in Fig. 3(c).

We now consider nuclear spins. The nuclear spin functions transform as follows:[18]

$$\text{for } NH_3:\ \Gamma(\Psi_{NS})=12A_1'+6E',$$
$$\text{for } ND_3:\ \Gamma(\Psi_{NS})=30A_1'+3A_2'+24E'. \quad (4)$$

According to the Pauli principle, the overall wave function must be antisymmetric with respect to permutation of two identical nuclei in the case of fermions, while it must be symmetric in the case of bosons. In the case of NH_3 (D_{3h} PI group), the Pauli-allowed total wave functions Ψ_{total} must transform as either A_2' or A_2''.[18] Therefore, for $k=0$ stacks, we note that only the A_2' or A_2'' Ψ_S levels can exist leaving only one inversion level (− for $\Sigma 0_0$ states and + for $\Pi 1_0$

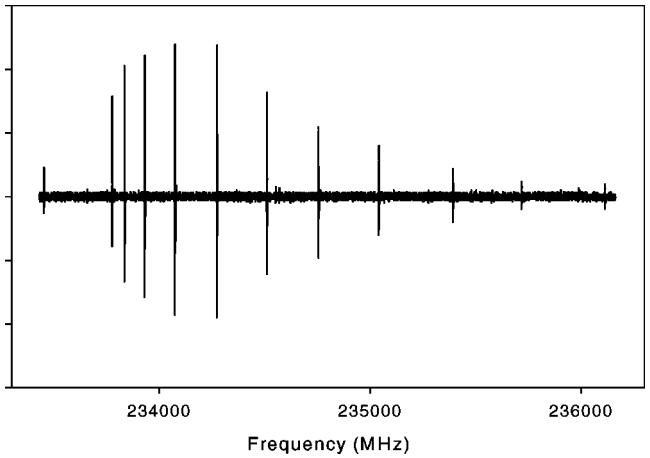

FIG. 4. Experimental spectrum of the *Q*-branch region of the $\Sigma 0_0 \rightarrow \Pi 1_0$ transition of $Ar \cdot ND_3$.

states) corresponding to the spin wave function $\Psi_{NS}(A_1')$, causing only one inversion component to be observed in the spectrum.

In the case of ND_3, the total wavefunction must transform as either A_1' or A_1''. Again, considering the results for Ψ_S in Fig. 3 we note that $\Psi_{\text{total}}(A_1', A_1'')$ can exist by combining $\Psi_S(A_1', A_1'')$ with $\Psi_{NS}(A')$ giving a statistical weight of 30, and also, by combining $\Psi_S(A_2', A_2'')$ with $\Psi_{NS}(A_2')$ giving a statistical weight of 3. The statistical weights of levels are marked on Fig. 3(c). Therefore two spectral components should be observed with relative intensities of 10:1. The dipole moment of the complex transforms according[6] to A_1'' thus allowing $A_1' \rightarrow A_1''$, $A_2' \rightarrow A_2''$, $E' \rightarrow E''$ transitions. Figure 3(c), shows the allowed transitions to the Π-bend in $Ar \cdot ND_3$.

Quantitatively the positions of the rotational levels, $E(J)$, are well represented by the following formulas[15] for each inversion component.

Σ states:

$$E(J) = B[J(J+1) - \Omega^2] - D[J(J+1) - \Omega^2]^2. \quad (5)$$

Π^- states:

$$E(J) = B[J(J+1) - \Omega^2] - D[J(J+1) - \Omega^2]^2 + q_\Omega J(J+1) + V_0.$$

Π^+ states:

$$E(J) = B[J(J+1) - \Omega^2] - D[J(J+1) - \Omega^2]^2 + V_0.$$

Here, B and D are the conventional rotational constants, V_0 is the origin of the Σ–Π bending vibration, and q_Ω is an Ω-doubling constant similar to the l-type doubling constant, which takes into account the rotational interaction of the $\Pi 1_0^-$ and $\Sigma 1_0$ states.

2. Experimental observations and fit

The search in the region near the predicted[3] $\Sigma 0_0 \rightarrow \Pi 1_0$ transition near 230 GHz revealed a total of 27 transitions assignable to *P*, *Q*, and *R* branches spanning the region from 195 to 263 GHz. The experimental spectrum of the *Q*-branch is shown on Fig. 4.

In addition, a second set of transitions falling into discernible *P*, *Q*, and *R* branches was found in the same region. These were about an order of magnitude less intense than the stronger ones and were assigned as transitions between the less populated inversion components. The separation between any two transitions with the same quantum numbers in the two sets was found to be nearly identical (about 2873 MHz). This value is consistent with the idea that the inversion potential is only modestly affected by complexation. The observed frequencies of all the transitions are given in Table III.

The two sets of lines, corresponding to the different inversion components, were fit separately to the pseudodiatomic model [Eqs. (5)] with a standard deviation of about 0.3 MHz. The resulting molecular constants are given in Table IV. The difference in the fit values of V_0 for the two inversion components yields $\Delta V_\Sigma + \Delta V_\Pi$, where ΔV_Σ and ΔV_Π refer to the inversion splitting of the Σ and Π levels, respectively. Assuming $\Delta V_\Sigma = \Delta V_\Pi = \Delta V$ yields a value of $\Delta V = 1436.2$ MHz compared with the 1591.8 MHz inversion splitting in the free monomer.

There is previous theoretical work[19,20] on the $Ar \cdot NH_3$ inversion potential. Also, the predicted energy levels of Schmuttenmaer *et al.*,[3] yield the tunneling splitting of the $Ar \cdot ND_3$ complex for the observed levels. Most interestingly this calculation yields a value of $\Delta V = 1448$ MHz, very similar to the observed value. We expect soon to report on experimental work[21] in progress on $Ne \cdot ND_3$ and $Kr \cdot ND_3$. At that point we will further compare the experimental observations with expectations from theoretical models of the inversion potential in the complexes.

If the two inversion components are treated as different species, the remaining molecular constants are very similar. A small difference in q_Ω accounts for the observed slight *J* dependency in the inversion separation in *P* and *R* branches (see Table III) which terminate on Π^- levels while in the *Q* branches that terminate on Π^+ levels, this separation is virtually *J* independent. At the present we are unsure of the precise mechanism leading to the weak *J* dependence in the inversion splitting of the Π^- levels.

The centrifugal distortion constants for Σ states in different inversion components differ by about two standard deviations of the fit. However, the small value of the difference in these constants and the lack of additional experimental data at high *J*, due to the low temperature of the sample, lead us not to speculate further concerning this difference.

Hyperfine structure was detected in the rotational lines of the $\Pi 1_0 \leftarrow \Sigma 0_0$ transition resulting from the quadrupole interaction of ^{14}N nucleus ($I = 1$) with the electric field gradient at the site of the nucleus. Low *J* transitions revealed several partially resolved components. Higher *J* lines ($J > 2$) were split into two components with an intensity ratio 2:1 and a separation by 1 MHz which was independent of *J* within experimental error.

For high *J*, the hyperfine components for which the change in *J* equals the change in the total angular momentum *F*, have maximum intensity.[22] This results in the predominance of three lines which are of comparable intensity and of which two are so close as to be unresolved by our experi-

TABLE III. Observed transitions and assignment of the $\Pi 1_0 \leftarrow \Sigma 0_0$ transition of Ar·ND_3.

		Upper inversion component		Lower inversion component		
J'	J''	Freq (MHz)	O–C (MHz)	Freq (MHz)	O–C (MHz)	Inversion splitting
1	0	238 833.7	−0.3	235 961.8	0.3	2871.9
2	1	243 871.3	−0.2	240 999.9	0.4	2871.4
3	2	248 823.9	−0.3	245 952.3	−0.7	2871.6
4	3	253 690.6	0.5	250 820.3	0.3	2870.3
5	4	258 466.9	0.1	255 598.3	0.0	2868.6
6	5	263 151.7	−0.2	260 285.7	0.0	2866.0
7	6	267 743.3	0.1			
1	2	223 231.0	−0.2	220 358.2	−0.3	2872.8
2	3	217 871.6	−0.4	215 000.3	0.3	2871.3
3	4	212 436.0	0.2	209 565.6	0.1	2870.4
4	5	206 924.2	−0.1	204 055.9	−0.1	2868.3
5	6	201 339.7	0.4	198 472.7	−0.1	2867.0
6	7	195 683.0	−0.3	192 816.7	0.0	2866.3
1	1	233 748.5	−0.4	230 876.0	0.0	2872.5
2	2	233 819.4	−0.1	230 946.6	0.0	2872.8
3	3	233 925.6	0.1	231 052.5	0.0	2873.1
4	4	234 067.6	0.3	231 194.1	0.0	2873.5
5	5	234 245.5	0.6	231 371.5	0.1	2874.0
6	6	234 458.9	0.1	231 585.4	0.1	2873.5
7	7	234 709.3	−0.1	231 835.9	0.0	2873.4
8	8	234 996.5	−0.7			
9	9	235 323.1	0.3			
10	10	235 686.7	−0.1			
11	11	236 090.1	0.1			
12	12	236 533.0	−0.2			
13	13	237 017.7	0.4			
14	14	237 543.1	−0.2			

ment. This accounts for the splitting and the 1:2 intensity ratio observed. Inspection of the formula that gives the quadrupole splitting shows that its J dependence decreases with increasing J.[22] A very similar splitting of transitions was observed by Zwart *et al.* in their work on Ar·NH_3.[7] Quadrupole coupling constants were fit to the two sets of transitions that gave rise to the 1 MHz splitting in the Q branch of the strong upper inversion component. The following expressions for level energies was used in the analysis:[7]

Σ states:

$$\mathcal{E}_{\mathcal{HFS}} = -eQq_{aa} f(I,J,F).$$

Π states:

$$\mathcal{E}_{\mathcal{HFS}} = \left(eQq_{aa} \frac{3 - J(J+1)}{J(J+1)} \pm \frac{1}{2} eQ(q_{bb} - q_{cc}) \right) \times f(I,J,F).$$

Here $f(I,J,F)$ is the Casimir function,[22] Q is the nuclear quadrupole moment of nitrogen, and the q_{ii} are values of the components of the electrical field tensor along the principle axes of rotation at the site of the nitrogen nucleus. The constants from the fit are presented in (c) of Table IV. The quadrupole constant eQq has been obtained from the fit and is the same as that reported for ND_3 (Ref. 23) within the error of the fit. Therefore there is no experimental evidence for an effect of molecular complexation on the quadrupole coupling constant.

TABLE IV. Molecular constants of Ar–ND_3.

	$\Sigma 0_0$	$\Pi^+ 1_0$	$\Pi^- 1_0$
	(a) Upper inversion component		
B (MHz)	2600.84(4)	2618.40(4)	
D (kHz)	64(1)	64(1)	72(1)
q_Ω (MHz)		−58.22(2)	
V_0 (MHz)		236 331.8(2)	
	(b) Lower inversion component		
B (MHz)	2600.93(5)	2618.35(4)	
D (kHz)	71(2)	65(1)	73(1)
q_Ω (MHz)		−58.02(2)	
V_0 (MHz)		233 459.4(2)	

(c) Quadrupole constants

	$\Sigma 0_0$	$\Pi 1_0$
eQq_{aa} (MHz)	0.9(5)	1.6(3)
$eQq_{bb} - eQq_{cc}$ (MHz)		−5.4(3)
eQq (MHz)[a]		−3.8(5)(−4.023)

[a]Value of the quadrupole coupling constant $eQq(q = q_{aa} + q_{bb} - q_{cc})$ deduced in the present experiment and in parentheses the value for eQq in free ND_3.

IV. CONCLUSION

A new submillimeter wave spectrometer has been developed for rapidly searching for new molecular transitions in a free supersonic jet environment. The apparatus is capable of detecting weakly absorbing and/or low abundance species. The apparatus has been used to observe the hindered rotation

transitions in Ar·CO and the vibration–rotation–inversion spectrum of the Π–Σ bend for $k=0$ in $Ar\cdot ND_3$, in the region 195–265 GHz. Molecular constants for the complex in the lowest two states have been obtained by fitting observed transition frequencies to a simple Hamiltonian. The upper $\Pi 1_0$ state was found to be perturbed by Coriolis interaction. The sum of the inversion splittings in the ground Σ and first excited Π states ($\Delta V_\Sigma + \Delta V_\Pi$) was found to be 2872.8 MHz. This is a little less than in the ND_3 monomer (3183.6 MHz) which indicates that the inversion motion of ND_3 is slightly hindered in the complex.

ACKNOWLEDGMENTS

We would like to thank Dr. Michael Pushkarsky for helpful discussions. We also would like to thank National Science Foundation for support of this work (Grants Nos. CHE-9974404 and CHE-0077974).

[1] D. T. Petkie, T. M. Goyette, R. P. A. Bettens, S. P. Belov, S. Albert, and F. C. De Lucia, Rev. Sci. Instrum. **68**, 1675 (1997).
[2] M. Hepp, W. Jager, and G. Winnewisser, J. Mol. Spectrosc. **176**, 58 (1996).
[3] C. A. Schmuttenmaer, R. C. Cohen, and R. J. Saykally, J. Chem. Phys. **101**, 146 (1994).
[4] C. Schmuttenmaer, R. Cohen, J. Loeser, and R. Saykally, J. Chem. Phys. **95**, 9 (1991).
[5] D. D. Nelson, G. T. Fraser, K. Zhao, F. J. Lovas, R. D. Suenram, and W. Klemperer, J. Chem. Phys. **85**, 5512 (1986).
[6] J. W. I. van Bladel, A. van der Avoird, and P. E. S. Wormer, J. Phys. Chem. **95**, 5414 (1991).
[7] E. Zwart and W. L. Meerts, Chem. Phys. **151**, 407 (1991).
[8] G. T. Fraser, D. D. Nelson, A. Charo, and W. Klemperer, J. Chem. Phys. **82**, 2535 (1985).
[9] G. Chalanski, S. M. Cybulski, M. M. Szczesniak, and S. Scheiner, J. Chem. Phys. **91**, 7809 (1989).
[10] M. Bulski, P. E. S. Wormer, and A. van der Avoird, J. Chem. Phys. **94**, 491 (1991).
[11] E. Zwart, H. Linnartz, W. L. Meerts, G. T. Fraser, D. D. Nelson, and W. Klemperer, J. Chem. Phys. **95**, 793 (1991).
[12] D. H. Gwo, M. Havenith, K. L. Busarow, R. C. Cohen, C. A. Schmuttenmaer, and R. J. Saykally, Mol. Phys. **71**, 453 (1990).
[13] J. W. I. van Bladel, A. van der Avoird, and P. E. S. Wormer, J. Chem. Phys. **94**, 501 (1991).
[14] C. A. Schmuttenmaer, J. G. Loeser, and R. J. Saykally, J. Chem. Phys. **101**, 139 (1994).
[15] Y. Xu and A. R. W. McKellar, Mol. Phys. **88**, 859 (1996).
[16] M. Hepp, R. Gendriesch, I. Pak, Y. A. Kuritcyn, F. Lewen, G. Winnewisser, M. Brookes, A. R. W. McKellar, J. K. G. Watson, and T. Amano, Mol. Phys. **92**, 229 (1997).
[17] L. Fusina and S. N. Murzin, J. Mol. Spectrosc. **167**, 464 (1994).
[18] P. R. Bunker and P. Jensen, *Molecular Symmetry and Spectroscopy* (NRC Research Press, Ottawa, Canada, 1998).
[19] J. W. I. van Bladel, A. van der Avoird, and P. E. S. Wormer, Chem. Phys. **165**, 47 (1992).
[20] G. Chalasiński, S. M. Cybulski, M. M. Szczęśniak, and S. Scheiner, J. Chem. Phys. **91**, 7809 (1989).
[21] D. G. Melnik, F. C. De Lucia, and T. A. Miller (unpublished).
[22] C. H. Townes and A. L. Schawlow, *Microwave Spectroscopy* (McGraw-Hill, New York, 1955).
[23] A. S. Bashkin, Opt. Spektrosk. **27**, 360 (1969).